A Multicomponent Visible-Light Initiating System for Rapid and Deep Photocuring through UV-Opaque Polyimide Films

Daihyun Hwang, Woojin Jeon, Seokju Lee, Shinya Onoue, Hyeon-Deuk Hwang, Johannes Gierschner, and Min Sang Kwon

A Multi-Component Visible-Light Initiating System for Rapid and Deep Photocuring through UV-opaque Polyimide Films

Daihyun Hwang,[1] Woojin Jeon,[1] Seokju Lee,[1] Onoue Shinya,[2] Hyeon-Deuk Hwang,[2]

Johannes Gierschner[3], and Min Sang Kwon[1,*]

[1]Department of Materials Science and Engineering, Research Institute of Advanced Materials, Seoul National University, Seoul 08826, Republic of Korea

[2]Samsung Display Co., Ltd., Yongin-si, Republic of Korea

[3]Madrid Institute for Advanced Studies, IMDEA Nanoscience, Calle Faraday 9, Campus Cantoblanco, Madrid, 28049, Spain

e-mail: minsang@snu.ac.kr (M.S.K.)

Abstract

Polyimides (PIs) play a crucial role in modern electronics, especially in flexible printed circuit boards (FPCBs). However, these FPCBs are vulnerable to physical damage, which can compromise the copper wiring. To protect this wiring, encapsulation with resin is commonly used. Traditional UV-curable resins, however, are ineffective due to the UV opacity of PI films, which hinders proper curing. In this study, we present an advanced multicomponent photoinitiating system, activated by visible light, that enables rapid and deep curing of acrylic resins even through UV-opaque PI films. This system, which integrates camphorquinone/amine (a well-established type II system) with a highly efficient triplet-generating photoredox catalyst and coinitiators, offers exceptional curing speed and depth. When tested on a real FPCB, the system achieved a curing depth exceeding 1 cm within just 10 s under 480 nm LED light, highlighting its practical value for intricate FPCB designs. We believe that this system will play a key role in a variety of applications that require fast and deep photocuring, such as 3D/4D printing.

Introduction

Polyimides (PIs) are high-performance polymer materials, highly esteemed for their excellent thermal stability, mechanical and chemical resilience, and electrical insulation, making them ideal for harsh environments[1,2]. These properties render PI essential in modern electronic devices[3,4]. Their remarkable thermal stability, in particular, makes them fundamental for mounting heat sinks in high-performance smartphones and mobile devices, addressing thermal issues[5,6,7,8]. In the electric vehicle sector, PIs are used as thermal management materials for batteries, preventing issues such as fires and contributing to sustained high performance[9]. Additionally, PI can achieve low dielectric constant through appropriate molecular structural optimization, which is beneficial for minimizing data loss in high-speed communication equipment like 5G[10,11,12]. PIs are particularly essential for flexible printed circuit boards (FPCBs) in modern electronic products with complex structures due to their high flexibility[13,14]. These boards feature intricate copper (Cu) wiring patterns to transmit electrical signals, with PI films serving as supporting substrates and insulators, ensuring that electricity flows along the intended circuit path (Fig. 1a). The high flexibility and stress resistance of PI films allow them to be easily bent, folded, and shaped into intricate forms, thereby maximizing space utilization[15,16,17]. However, issues arise when the FPCB, particularly in sections that are bent and exposed, is subjected to physical impact, which can deform the FPCB and damage the Cu wiring.

Wrapping the Cu wiring in these bent sections with a resin possessing excellent mechanical properties can protect them from physical impact and deformation[18]. However, conventional UV-curable resins are unsuitable for this purpose because the UV opacity of the PI film prevents curing of the resin located inside (Fig. 1b)[19,20]. While thermal curing is an alternative, it risks damaging other components and is slower than photocuring, making it less preferred in the industry[21]. We hypothesize that this issue can be resolved by using a photoinitiation system that operates efficiently under visible light, which can penetrate the UV-opaque PI film. However, to date, no study has been reported on an optimized visible-light initiation system designed for photocuring through UV-opaque PI films.

We here present a multicomponent photoinitiating system that allows rapid and deep photocuring of acrylic resins through UV-opaque PI films under blue LED irradiation. To achieve our objectives, we employed a following strategy: i) We utilized camphorquinone/amine, a well-established type II photoinitiating system already commercialized, as the primary photoinitiator. ii) To address the challenges of slow curing speed and inadequate curing depth inherent to this camphorquinone/amine, we incorporated a mixture of the 4DP-IPN/borate/iodonium, a recently developed high-efficiency photoredox catalyst-based photoinitiating system. Our analysis revealed that this multicomponent system demonstrated superior initial curing speed and conversion under blue LED irradiation. It significantly outperformed the individual use of camphorquinone/amine or 4DP-IPN/borate/iodonium in terms of initial curing rate, conversion and curing depth. Mechanistic studies suggest that this superior performance is driven by efficient Dexter-type energy transfer between 4DP-IPN and camphorquinone, as well as electron transfer between camphorquinone and borate/iodonium. When applied to an actual FPCB, the system achieved a curing depth of over 1 cm in just 10 seconds under intense 480 nm LED irradiation (1000 mW/cm²), confirming its practical utility for high-curvature FPCB applications. We believe that this system will play a key role in a variety of applications that require fast and deep photocuring, such as 3D/4D printing.

RESULTS AND DISCUSSION

Design of the system

The advent of energy-efficient, narrow spectral width LED-based light sources has enabled effective photocuring in both the visible

and UV ranges[22,23]. Visible-light curing, in particular, overcomes the limitations of conventional UV curing, such as low cure depth due to high UV-absorption/-scattering in most materials, and potential harm to DNA and cells[24,25,26,27,28]. Consequently, there has been a significant increase in interest in photoinitiating systems activated by visible-light over the past decade, leading to their use in various applications such as dental resins, 3D/4D printing, coatings, adhesives, paints, sealants, and resist materials[29,30,31,32,33,34].

In visible-light curing, an efficient photoinitiation system is essential. A notable example is the camphorquinone/amine system, a type II curing agent commercialized in the 1970s (Fig. 1c)[35,36,37,38,39,40]. This system absorbs light at 468 nm, enabling it to cure through polyimide. However, its slow initial reaction speed, due to limited rate of hydrogen abstraction, poses a drawback. Increasing the amount used to enhance the reaction speed results in decreased curing depth[41]. In contrast, type I systems, such as BAPO and TPO (phosphine oxides), offer faster curing speeds and have been commercialized for various applications (Fig. 1c). Despite their advantages, these systems struggle to cure through polyimide because their absorption is insufficient at around 420 nm (Supplementary Fig. 6). For such applications, type I systems with longer absorption wavelengths are required. Although several new systems have been developed recently[42], they often involve relatively complex synthesis processes. Moreover, for type I photoinitiators, the decomposition rate is critical; a slower rate requires higher concentrations for rapid curing, which reduces light transmittance and limits curing depth. Additionally, it lacks oxygen tolerance compared to camphorquinone/amine or photoredox catalyst-based photoinitiating systems[43,44].

Recently, numerous studies have focused on visible light curing systems composed of photoredox catalysts and coinitiators[45,46,47,48]. Our team has developed several such systems based on cyanoarene-based photoredox catalysts[49,50,51,52,53,54], successfully applying them to a range of organic reactions and polymerizations[55,56,57]. Originally proposed by the Adachi group as thermally activated delayed fluorescence (TADF) emitters for high-efficiency OLED applications[58], cyanoarene-based donor-acceptor molecules can be customized to optimize various photoredox reactions, as their redox potential is easily controlled by adjusting the donor and acceptor components[59,60]. Cyanoarene-based materials are particularly efficient because they utilize a long-lived triplet excited state, enabling photoredox catalysts to proceed efficiently even in very small amounts. This makes them ideal for photocuring resins that require transparency or deep curing. A representative cyanoarene-based catalyst, 4DP-IPN, absorbs light up to 500 nm and has an excited-state triplet lifetime exceeding 100 μs, making it an excellent visible-light photocatalyst (Fig. 1d, e)[61]. Our recent study demonstrated that when iodonium and borate are used as coinitiators, electron transfer with 4DP-IPN is rapid, forming an effective photoinitiation system for visible light[62].

Building on these findings, we combined camphorquinone/amine as a primary photoinitiator with a mixture of 4DP-IPN/borate/iodonium to address issues of slow curing speed and inadequate curing depth. We selected ethyl 4-(dimethylamino)benzoate (EDB) as the amine to prevent cross-reaction with the 4DP-IPN/borate/iodonium system and ensure sufficient oxygen tolerance. The acrylic resin used for evaluation was a mixture of bisphenol A-glycidyl methacrylate (Bis-GMA) and N,N-Dimethyl acrylamide (DMAA) in a 60:40 weight ratio (Fig. 2a). This combination was chosen for its excellent mechanical properties, making it ideal for protecting FPCBs[63].

Kinetics of photocuring in multicomponent systems

Each photoinitiating system was initially optimized through kinetics monitoring (Fig. 2b−d). For kinetics experiments, films were prepared by coating an acrylic resin containing each photoinitiating system between two silicone-treated 100 μm thick polyethylene terephthalate films (Youngwoo Trading) to a thickness of 50 μm. These films were then cured using a 450 nm LED lamp at an intensity of 10 mW/cm² (Fig. 2a). The conversion was analyzed using FT-IR spectroscopy by measuring the decrease in the C=C double bond at 790 cm^{-1} of the acryl group, relative to the C=O bond at 1720 cm^{-1}, which remains unaffected by the curing process.

To optimize the amount and ratio of the catalyst and each co-initiator in the 4DP-IPN/borate/iodonium system, a photocuring experiment with acrylic resin was conducted. The kinetics were monitored by varying the PC content (10, 25, 50 ppm) while maintaining the borate and iodonium contents at 3000 ppm and 5000 ppm, respectively (Fig. 2b). The results indicated that the initial conversion rate increased with higher PC content, with no significant difference between 25 ppm and 50 ppm. Subsequently, the PC content was fixed at 25 ppm, and the kinetics was compared by varying the borate and iodonium contents (Fig. 2c). The results showed that the initial rate increased with higher co-initiator content, with minimal difference between the conditions of borate 1800 ppm, iodonium 3000 ppm, and borate 3000 ppm, iodonium 5000 ppm. Thus, the optimal conditions were determined to be 4PD-IPN 25 ppm, borate 1800 ppm, and iodonium 3000 ppm.

Subsequently, the CQ/EDB system was evaluated, with the kinetics monitored by varying the CQ content while keeping the EDB content at six times the molar amount of CQ (Fig. 2d)[64]. As the CQ concentration increased, both the initial reaction rate and the final conversion improved. The initial rate, however, was considerably slower than that of the 4DP-IPN/borate/iodonium system, although the final conversion was slightly higher. Under optimized conditions, the 4DP-IPN/borate/iodonium system achieved approximately 60% conversion within 10 seconds, after which no further conversion occurred despite prolonged curing. In contrast, the CQ/EDB system reached around 20% conversion in 10 seconds and approximately 80% conversion in 300 seconds at a CQ concentration of 4000 ppm.

As anticipated, the two systems exhibited distinctly different kinetics. The 4DP-IPN/borate/iodonium system displayed a rapid initial rate but quickly reached saturation. In contrast, the CQ/EDB system had a slower initial rate but continued to increase gradually until saturation. To harness the advantages of both photoinitiating systems, a multicomponent system was proposed. This system comprised a 4DP-IPN/borate/iodonium component reduced to one-third of its original concentration (PC 10 ppm, borate 600 ppm, and iodonium 1000 ppm) and a CQ/EDB component halved in concentration (CQ 2000 ppm, EDB 12000 ppm). As shown in Fig. 2e, the combined system exhibited an initial rate as rapid as the 4DP-IPN/borate/iodonium system. As the curing time progressed, the conversion rate increased gradually, akin to the CQ/EDB system. These kinetic patterns are expected to meet the practical requirements for both rapid and thorough curing. Additionally, this approach is economically advantageous, as it significantly reduces the need for the relatively expensive 4DP-IPN/borate/iodonium component.

Photocuring penetrated through PI film using the multicomponent system

Next, we investigated the efficacy of the developed multicomponent photoinitiating system in penetrating PI film to effectively cure acrylic resin. For the kinetics experiments, an acrylic resin with a photoinitiation system was coated between two 100 μm thick silicone-treated PET films to produce a 50 μm thick film (Fig. 2a). A 25 μm thick DuPont™ Kapton® PI film was then placed on top, and a photocuring experiment was conducted using a 450 nm LED lamp at an intensity of 10 mW/cm². As expected, a significant decrease in curing speed was observed due to the PI film's transmittance of approximately 0.35% at 450 nm. Under optimized conditions, the multicomponent photoinitiating system achieved about 30% conversion in 60 seconds and 60% conversion in 300 seconds (Fig. 2f). This was still much faster than the 4DP-IPN/borate/iodonium system or the CQ/EDB system.

To further increase the curing speed, we switched the light source to 480 nm, where the photoinitiating system has higher absorption and the PI film shows better transmittance (approximately 7.3% at 480 nm). As anticipated, the multicomponent system's initial curing speed was significantly higher with the 480 nm light source, achieving approximately 55% conversion in 60 seconds, and again surpassing the 4DP-IPN/borate/iodonium and CQ/EDB systems (Fig. 2g). In summary, a light source of 450 nm results in substantial light blockage by the PI film, leading to slower curing speeds compared to when no PI film is present. However, using a 480 nm LED and increasing light source intensity with the multicomponent photoinitiating system can achieve a curing speed

suitable for practical applications.

Curing depth assessment of resin

FPCBs can be bent into various curvatures based on the shape and position of the electronic substrate, increasing the required distance for resin curing as the curvature grows (Fig. 1b). This elongates and complicates the curing pathway, making both rapid curing and deep curing depth crucial. The depth curing performance may vary depending on the type of initiator system used. It was anticipated that longer-wavelength visible light would enhance depth curing by increasing transmittance through the PI film and resin[65].

To assess the cure depth for each photoinitiating system, a black tube with a height of 30 mm and a width of 6 mm was used to block light (Fig. 3a). This tube was vertically positioned and filled with resin containing one of the three systems: the multicomponent system, the 4DP-IPN/borate/iodonium system, or the CQ/EDB system. The tube was then covered with a 25 μm thick PI film and exposed to 450 nm and 480 nm light at an intensity of 10 mW/cm². Curing proceeded vertically, and after completion, the uncured liquid was removed and the depth of the cured portion was measured.

The overall pattern of the experiments on curing depth closely mirrored that of the curing speed. As shown in Fig. 3b, under 450nm irradiation, the curing speed was extremely slow. During the 3-minute curing period, none of the three systems showed any signs of curing. At curing times of 5 and 10 minutes, the multicomponent system achieved curing depths of approximately 0.3 cm and 0.7 cm, respectively. The 4DP-IPN/borate/iodonium system showed curing depths of 0.15 cm and 0.4 cm, while the CQ/EDB system showed no curing at 5 minutes and a curing depth of approximately 0.25 cm at 10 minutes. In contrast, the 480nm irradiation exhibited significantly improved curing behavior (Fig. 3c). The multicomponent system cured to a depth of 0.25 cm in 1 minute and nearly 2 cm in 10 minutes, demonstrating much deeper curing than both the 4DP-IPN/borate/iodonium and CQ/EDB systems. Interestingly, the curing depth increased linearly with time, indicating a consistent curing speed regardless of depth, and suggesting minimal light intensity attenuation with depth. This efficiency is attributed to the multicomponent system's highly effective photoinitiation, requiring only a small amount to achieve sufficient curing with minimal light absorption. When the light intensity was increased to 1000 mW/cm², the curing pattern remained similar, but the curing speed increased significantly (Fig. 3d). Under 480nm irradiation, the multicomponent system achieved curing depths of 0.8 cm in 5 seconds and nearly 2.5 cm in 1 minute, representing a tenfold increase in speed compared to a light intensity of 10 mW/cm².

Evaluation of the multicomponent system in simulated FPCB environments

Finally, to evaluate the practicality of the multicomponent system for an actual FPCB, we conducted an experiment under conditions simulating real-life applications (Fig. 4a and Supplementary Fig. 7). The FPCB was constructed with 12.5μm thick PI films on the top and bottom, 100μm wide Cu wiring spaced 100μm apart, and a 10μm thick adhesive layer. It was then bent to a radius of 3mm and placed in a silicone mold for resin injection. An acrylic resin containing the multicomponent system was injected into the bent FPCB, and the mold was sealed to prevent resin leakage, with resin also applied to the exposed edges of the FPCB. The resin was exposed to 450 nm or 480 nm LED light at an intensity of 1000 mW/cm² for curing. After light exposure, the FPCB was removed, the uncured resin was washed off, and the depth of the cured resin was measured over time (Fig. 4b). As anticipated, the curing behavior at 480nm was significantly superior to that at 450nm, achieving a depth of 0.8 cm in 5 seconds and approximately 2 cm in 30 seconds. This highlights the substantial potential of the multicomponent photoinitiating system developed in this study for real-world applications.

Photoinitiating mechanism of a multicomponent system

To elucidate the origin of the multicomponent system's excellent performance, we examined its photoinitiating mechanism in detail. We began by conducting a Stern-Volmer experiment, analyzing photoluminescence (PL) decay quenching of 4DP-IPN in the presence of other components (Fig. 5b). To simulate the actual curing environment, DMAc was used as the solvent due to its polarity, which closely resembles that of the monomer, DMAA. Notably, camphorquinone exhibited a very high quenching rate (k_q = 2.4 x 10^8 $M^{-1}s^{-1}$), approximately ten times that of iodonium (k_q = 2.1 x 10^7 M^{-1s-1}). Borate displayed a much slower quenching rate (k_q = 3.2 x 10^4 M^{-1s-1}), while almost no quenching was observed for EDB. These findings suggest that, contrary to our initial assumption, the camphorquinone/EDB system and the 4DP-IPN/borate/iodonium system do not function entirely independently.

To investigate the PL quenching mechanism of 4DP-IPN in the presence of camphorquinone, we measured the redox potentials and triplet energies of both compounds, supplementing our data with literature values when direct measurements were challenging (Supplementary Table 1). These parameters indicated that both electron and energy transfer processes were feasible. Additionally, we measured the quenching rates between camphorquinone and 4Cz-IPN and 4DCDP-IPN, which possess higher triplet energies but lower excited-state reduction potentials compared to 4DP-IPN (Supplementary Table 1). The higher quenching rates for 4Cz-IPN (k_q = 3.1 x 10^8 $M^{-1\ s-1}$) and 4DCDP-IPN (k_q = 2.7 x 10^8 $M^{-1\ s-1}$), while still below the diffusion limit (6.1 x 10^9 $M^{-1\ s-1}$)[66], exceed that of 4DP-IPN. This indicates that the quenching between 4DP-IPN and camphorquinone likely occurs through triplet–triplet energy transfer. However, given the complexity of Dexter-type energy transfer, the electron transfer mechanism cannot be entirely ruled out, warranting further investigation.

Building on these findings and the redox potentials of the other components (iodonium, borate, EDB), we propose the following mechanism (Fig. 5a and Supplementary Fig. 9): both 4DP-IPN and camphorquinone absorb light, with similar absorption efficiency given their comparable extinction coefficients. Upon absorbing light, 4DP-IPN rapidly transfers its energy to camphorquinone, generating its triplet state. While camphorquinone may undergo a Type II reaction with EDB, the electron transfer and hydrogen abstraction processes are relatively slow, limiting the reaction speed. Instead, a rapid electron transfer from borate to camphorquione leads to bond dissociation and the formation of an initiating radical. The camphorquinone radical anion intermediate is regenerated to camphorquinone through electron transfer to iodonium, which, upon accepting the electron, undergoes bond dissociation to produce an initiating radical. This cycle allows for the consumption of iodonium and borate without significantly depleting 4DP-IPN or camphorquinone. Once sufficient consumption has occurred, the Type II reaction between camphorquinone and EDB, sensitized by 4DP-IPN, becomes the dominant reaction pathway.

CONCLUSIONS

High-performance polymer materials, such as PI film, play a crucial role in numerous industrial sectors, including electric vehicle batteries, smartphones, OLED panels, and high-speed communication equipment. The flexibility of PI film makes it an indispensable component of FPCBs, which connect circuits in various electronic devices and need protection against physical impact and deformation. Traditional UV curing systems are ineffective due to the UV opacity of PI film. To address this, a novel multicomponent photoinitiating system was developed for rapid and deep photocuring of acrylic resins through UV-opaque PI films under visible-light irradiation. By combining camphorquinone/amine with 4DP-IPN/borate/iodonium, the system demonstrated superior curing speed and depth, proving highly effective for high-curvature FPCB applications. It significantly outperformed the individual use of camphorquinone/amine or 4DP-IPN/borate/iodonium in initial curing rate, conversion, and curing depth. The multicomponent system showed excellent initial speed and final conversion performance under both 450 nm and 480 nm visible light. Curing depth

assessments revealed greater curing depths with extended light exposure, particularly at 480 nm. Application to actual FPCBs confirmed effective deep curing, even in high-curvature configurations, indicating reliable performance. Additionally, the dual system reduces the high cost of traditional PC systems, enhancing its industrial applicability and potential. This study demonstrated that visible light-curing technology effectively cures internal resins within UV-opaque films like PI film across various industrial applications, significantly improving durability and safety in diverse industrial fields.

Methods

General experimental procedures for film polymerization. The resin used in the experiment was a mixture of BisGMA and DMAA at a 60:40 weight ratio. Prior to mixing, the photoinitiator, co-initiator, and PC were first dispersed in the DMAA. The resin mixture was coated between two sheets of polyethylene terephthalate (silicon-treated PET film, 100 μm, Youngwoo Trading). The resin thickness was precisely controlled to 50 μm using a film applicator. Following this, the film was placed into LED curing equipment and exposed to light at wavelengths of 450 nm and 480 nm for various durations, with an intensity set at 10mW/cm². Curing evaluations were conducted on films both covered and uncovered with a PI film to assess the curing rate post PI transmission.

General experimental procedures for curing depth assessment. To assess the cure depth of each photoinitiating system, a black tube with a height of 30 mm and a width of 6 mm was vertically positioned and filled with resin. The resin contained one of three systems: the multicomponent system, the 4DP-IPN/borate/iodonium system, or the CQ/EDB system. A PI film 25 μm thick was then placed over the top, allowing light projected from above to pass through the PI and irradiate the resin. The resin was exposed to light at wavelengths of 450 nm and 480 nm with an intensity of 10 mW/cm². The curing process was conducted vertically, and after completion, any remaining uncured resin was removed to measure the depth of the resin that had successfully cured.

General experimental procedures for curing depth assessment in simulated actual FPCB. To determine the curing depth for an actual FPCB, an FPCB with layers of 12.5μm PI films on both surfaces, copper wires 100μm wide and spaced 100μm apart, and a 10μm adhesive layer was fabricated. A custom silicone mold was designed to mimic the real-world form of the FPCB. This FPCB was then curved into a 3mm radius and placed within the silicone mold, where a multicomponent acrylic resin was injected. The mold was tightly sealed to avoid any leakage of the resin, which was also applied to any exposed edges of the FPCB. Exposure to LED light at 450 nm and 480 nm wavelengths at an intensity of 1000 mW/cm² was used for curing. Following this procedure, the FPCB was extracted from the mold, any uncured resin was cleaned off, and the depth of the resin that had cured was measured.

Data Availability

The authors declare that the data supporting the findings of this study are available within the paper and its Supplementary Information.

References

1. Abadie M. *High performance polymers-polyimides based: from chemistry to applications*. BoD–Books on Demand (2012).
2. Qu C, Hu J, Liu X, Li Z, Ding Y. Morphology and mechanical properties of polyimide films: the effects of UV irradiation on microscale surface. *Materials* **10**, 1329 (2017).
3. Gouzman I, Grossman E, Verker R, Atar N, Bolker A, Eliaz N. Advances in polyimide-based materials for space applications. *Advanced materials* **31**, 1807738 (2019).
4. Sezer Hicyilmaz A, Celik Bedeloglu A. Applications of polyimide coatings: A review. *SN Applied Sciences* **3**, 363 (2021).
5. Li Y, *et al.* Boosting the heat dissipation performance of graphene/polyimide flexible carbon film via enhanced through-plane conductivity of 3D hybridized structure. *Small* **16**, 1903315 (2020).
6. Hsiao Y-S, *et al.* Lightweight flexible polyimide-derived laser-induced graphenes for high-performance thermal management applications. *Chemical Engineering Journal* **451**, 138656 (2023).
7. Li H, *et al.* Enhanced thermal conductivity of graphene/polyimide hybrid film via a novel "molecular welding" strategy. *Carbon* **126**, 319-327 (2018).
8. Fan D, Jin M, Wang J, Liu J, Li Q. Enhanced heat dissipation in graphite-silver-polyimide structure for electronic cooling. *Applied Thermal Engineering* **168**, 114676 (2020).
9. Lyu H, *et al.* Aromatic polyimide/graphene composite organic cathodes for fast and sustainable lithium-ion batteries. *ChemSusChem* **11**, 763-772 (2018).
10. Liu Y, Zhao X-Y, Sun Y-G, Li W-Z, Zhang X-S, Luan J. Synthesis and applications of low dielectric polyimide. *Resources chemicals and materials* **2**, 49-62 (2023).
11. Zhang C, He X, Lu Q. Polyimide films with ultralow dielectric loss for 5G applications: Influence and mechanism of ester groups in molecular chains. *European Polymer Journal* **200**, 112544 (2023).
12. Zhou Y. Material foundation for future 5G technology. *Accounts of Materials Research* **2**, 306-310 (2021).
13. Ni H-j, Liu J-g, Wang Z-h, Yang S-y. A review on colorless and optically transparent polyimide films: Chemistry, process and engineering applications. *Journal of Industrial and Engineering Chemistry* **28**, 16-27 (2015).
14. Yi C, *et al.* High-temperature-resistant and colorless polyimide: Preparations, properties, and applications. *Solar Energy* **195**, 340-354 (2020).
15. Jung H-S, Eun K, Lee E-K, Jung K-Y, Choi S-H, Choa S-H. Flexible Durability of Ultra-Thin FPCB. *Journal of the Microelectronics and Packaging Society* **21**, 69-76 (2014).
16. Kim BS, Bae SH, Park Y-H, Kim J-h. Polyimide/carbon nanotubes composite films: a potential for FPCB. In: *2006 International Conference on Nanoscience and Nanotechnology*). IEEE (2006).
17. Ratchev S. *Smart Technologies for Precision Assembly: 9th IFIP WG 5.5 International Precision Assembly Seminar, IPAS 2020, Virtual Event, December 14–15, 2020, Revised Selected Papers*. Springer Nature (2021).
18. Wang X, Tang F, Qi X, Lin Z. Mechanical, electrochemical, and durability behavior of graphene nano-platelet loaded epoxy-

resin composite coatings. *Composites Part B: Engineering* **176**, 107103 (2019).

19. French R, *et al.* Optical properties of materials for concentrator photovoltaic systems. In: *2009 34th IEEE Photovoltaic Specialists Conference (PVSC)*). IEEE (2009).

20. Reit R, Espinoza J, Vega A, Voutsas T, Avendaño-Bolívar A, Arreaga-Salas D. 82-3: Temporary Bonding Alternative to Laser Lift-Off for Flexible Displays. In: *SID Symposium Digest of Technical Papers*). Wiley Online Library (2018).

21. Chandra R, Soni R. Recent developments in thermally curable and photocurable systems. *Progress in polymer science* **19**, 137-169 (1994).

22. Xiao P, *et al.* Visible light sensitive photoinitiating systems: Recent progress in cationic and radical photopolymerization reactions under soft conditions. *Progress in Polymer Science* **41**, 32-66 (2015).

23. Dietlin C, *et al.* Photopolymerization upon LEDs: new photoinitiating systems and strategies. *Polymer Chemistry* **6**, 3895-3912 (2015).

24. Tasdelen MA, Lalevée J, Yagci Y. Photoinduced free radical promoted cationic polymerization 40 years after its discovery. *Polymer Chemistry* **11**, 1111-1121 (2020).

25. Topa M, Ortyl J. Moving towards a finer way of light-cured resin-based restorative dental materials: Recent advances in photoinitiating systems based on iodonium salts. *Materials* **13**, 4093 (2020).

26. Dumur F. Recent advances on photobleachable visible light photoinitiators of polymerization. *European Polymer Journal* **186**, 111874 (2023).

27. Armstrong BK, Kricker A. The epidemiology of UV induced skin cancer. *Journal of photochemistry and photobiology B: Biology* **63**, 8-18 (2001).

28. De Gruijl F. Skin cancer and solar UV radiation. *European journal of cancer* **35**, 2003-2009 (1999).

29. Abdallah M, *et al.* Acridone derivatives as high performance visible light photoinitiators for cationic and radical photosensitive resins for 3D printing technology and for low migration photopolymer property. *Polymer* **159**, 47-58 (2018).

30. Borjigin T, *et al.* The Blue-LED-Sensitive Naphthoquinone-Imidazolyl Derivatives as Type II Photoinitiators of Free Radical Photopolymerization. *Advanced Materials Interfaces* **10**, 2202352 (2023).

31. Chung K-Y, Page ZA. Boron-methylated dipyrromethene as a green light activated type I photoinitiator for rapid radical polymerizations. *Journal of the American Chemical Society* **145**, 17912-17918 (2023).

32. Lu P, *et al.* Wavelength-selective light-matter interactions in polymer science. *Matter* **4**, 2172-2229 (2021).

33. Kalout H, Lansalot M, Bourgeat-Lami E, Morlet-Savary F, Lacôte E, Lalevée J. A Methylene Blue/Sodium Sulfinate Photo-Initiating System for the Red-Light Emulsion Photopolymerization of Methyl Methacrylate. *Advanced Functional Materials*, 2406299 (2024).

34. Dumur F. Recent Advances in Monocomponent Visible Light Photoinitiating Systems Based on Sulfonium Salts. *Polymers* **15**, 4202 (2023).

35. Albuquerque PPA, Bertolo ML, Cavalcante LM, Pfeifer C, Schneider LF. Degree of conversion, depth of cure, and color stability of experimental dental composite formulated with camphorquinone and phenanthrenequinone photoinitiators.

Journal of Esthetic and Restorative Dentistry **27**, S49-S57 (2015).

36. Miletic V. *Dental composite materials for direct restorations*. Springer (2018).

37. Moszner N, Fischer UK, Ganster B, Liska R, Rheinberger V. Benzoyl germanium derivatives as novel visible light photoinitiators for dental materials. *Dental Materials* **24**, 901-907 (2008).

38. Ikemura K, Endo T. A review of the development of radical photopolymerization initiators used for designing light-curing dental adhesives and resin composites. *Dental Materials Journal* **29**, 481-501 (2010).

39. Kamoun EA, Winkel A, Eisenburger M, Menzel H. Carboxylated camphorquinone as visible-light photoinitiator for biomedical application: Synthesis, characterization, and application. *Arabian Journal of Chemistry* **9**, 745-754 (2016).

40. Santini A, Gallegos IT, Felix CM. Photoinitiators in dentistry: a review. *Primary dental journal* **2**, 30-33 (2013).

41. Kowalska A, Sokolowski J, Bociong K. The photoinitiators used in resin based dental composite—a review and future perspectives. *Polymers* **13**, 470 (2021).

42. Müller SM, Schlögl S, Wiesner T, Haas M, Griesser T. Recent advances in type I photoinitiators for visible light induced photopolymerization. *ChemPhotoChem* **6**, e202200091 (2022).

43. Segurola J, Allen N, Edge M, Roberts I. Photochemistry and photoinduced chemical crosslinking activity of acrylated prepolymers by several commercial type I far UV photoinitiators. *Polymer degradation and stability* **65**, 153-160 (1999).

44. Nie J, *et al.* Effect of peroxides and hydroperoxides on the camphorquinone-initiated photopolymerization. *Macromolecular Chemistry and Physics* **200**, 1692-1701 (1999).

45. Al Mousawi A, *et al.* Carbazole derivatives with thermally activated delayed fluorescence property as photoinitiators/photoredox catalysts for LED 3D printing technology. *Macromolecules* **50**, 4913-4926 (2017).

46. Sun K, Xiao P, Dumur F, Lalevée J. Organic dye-based photoinitiating systems for visible-light-induced photopolymerization. *Journal of Polymer Science* **59**, 1338-1389 (2021).

47. Quint V, Morlet-Savary F, Lohier J-F, Lalevee J, Gaumont A-C, Lakhdar S. Metal-free, visible light-photocatalyzed synthesis of benzo [b] phosphole oxides: synthetic and mechanistic investigations. *Journal of the American Chemical Society* **138**, 7436-7441 (2016).

48. Uddin A, *et al.* Do The Twist: Efficient Heavy-Atom-Free Visible Light Polymerization Facilitated by Spin-Orbit Charge Transfer Inter-system Crossing. *Angewandte Chemie International Edition* **62**, e202219140 (2023).

49. Jeon W, Kwon Y, Kwon MS. Highly efficient dual photoredox/copper catalyzed atom transfer radical polymerization achieved through mechanism-driven photocatalyst design. *Nature Communications* **15**, 5160 (2024).

50. Singh VK, *et al.* Highly efficient organic photocatalysts discovered via a computer-aided-design strategy for visible-light-driven atom transfer radical polymerization. *Nature Catalysis* **1**, 794-804 (2018).

51. Song Y, *et al.* Organic Photocatalyst for ppm-Level Visible-Light-Driven Reversible Addition–Fragmentation Chain-Transfer (RAFT) Polymerization with Excellent Oxygen Tolerance. *Macromolecules* **52**, 5538-5545 (2019).

52. Lee Y, Boyer C, Kwon MS. Photocontrolled RAFT polymerization: past, present, and future. *Chemical Society Reviews* **52**, 3035-3097 (2023).

53. Back J-H, Kwon Y, Kim H-J, Yu Y, Lee W, Kwon MS. Visible-light-curable solvent-free acrylic pressure-sensitive adhesives via photoredox-mediated radical polymerization. *Molecules* **26**, 385 (2021).

54. Back J-H, *et al.* Synthesis of solvent-free acrylic pressure-sensitive adhesives via visible-light-driven photocatalytic radical polymerization without additives. *Green Chemistry* **22**, 8289-8297 (2020).

55. Park Y, Kim J, Ahn D, Yu Y, Lee W, Kwon MS. Biomass-derived optically clear adhesives for foldable displays. *ChemSusChem*, e202301795 (2024).

56. Back JH, *et al.* Visible-Light-Curable Acrylic Resins toward UV-Light-Blocking Adhesives for Foldable Displays. *Advanced Materials* **35**, 2204776 (2023).

57. Kim D, *et al.* Ultraviolet light debondable optically clear adhesives for flexible displays through efficient visible-light curing. *Advanced Materials* **36**, 2309891 (2024).

58. Uoyama H, Goushi K, Shizu K, Nomura H, Adachi C. Highly efficient organic light-emitting diodes from delayed fluorescence. *Nature* **492**, 234-238 (2012).

59. Lee Y, *et al.* A water-soluble organic photocatalyst discovered for highly efficient additive-free visible-light-driven grafting of polymers from proteins at ambient and aqueous environments. *Advanced Materials* **34**, 2108446 (2022).

60. Yu C, *et al.* Silver sulfide nanocrystals as a biocompatible and full-spectrum photocatalyst for efficient light-driven polymerization under aqueous and ambient conditions. *ACS Catalysis* **13**, 665-680 (2022).

61. Kwon Y, *et al.* Formation and degradation of strongly reducing cyanoarene-based radical anions towards efficient radical anion-mediated photoredox catalysis. *Nature Communications* **14**, 92 (2023).

62. Kwon Y, *et al.* Ultraviolet light blocking optically clear adhesives for foldable displays via highly efficient visible-light curing. *Nature Communications* **15**, 2829 (2024).

63. Fugolin AP, Dobson A, Mbiya W, Navarro O, Ferracane JL, Pfeifer CS. Use of (meth) acrylamides as alternative monomers in dental adhesive systems. *Dental Materials* **35**, 686-696 (2019).

64. Neumann MG, Schmitt CC, Horn Jr MA. The effect of the mixtures of photoinitiators in polymerization efficiencies. *Journal of applied polymer science* **112**, 129-134 (2009).

65. Shao J, Huang Y, Fan Q. Visible light initiating systems for photopolymerization: status, development and challenges. *Polymer Chemistry* **5**, 4195-4210 (2014).

66. Lattke YM, Corbin DA, Sartor SM, McCarthy BG, Miyake GM, Damrauer NH. Interrogation of O-ATRP activation conducted by singlet and triplet excited states of phenoxazine photocatalysts. *The Journal of Physical Chemistry A* **125**, 3109-3121 (2021).

Acknowledgements

This research was supported by the Nano & Material Technology Development Program through the National Research Foundation of Korea(NRF) funded by Ministry of Science and ICT(RS-2024-00452255). It was also backed by Samsung Display Co., Ltd.

Author contributions

D.H. and M.S.K. were responsible for the initial conception of the project and wrote the initial draft of the manuscript. D.H. and W.J. performed the photophysical measurements and CV measurements. D.H., S.L. conducted the curing evaluation. D.H, W.J, S.L, S.O., H.H. and M.S.K discussed the curing test result. D.H., W.J., J.G., and M.S.K. were involved in the discussion of the photophysics and photochemical reactions. All the authors discussed the results and commented on the manuscript. M.S.K. supervised the project.

Competing interests

The authors declare no competing interests.

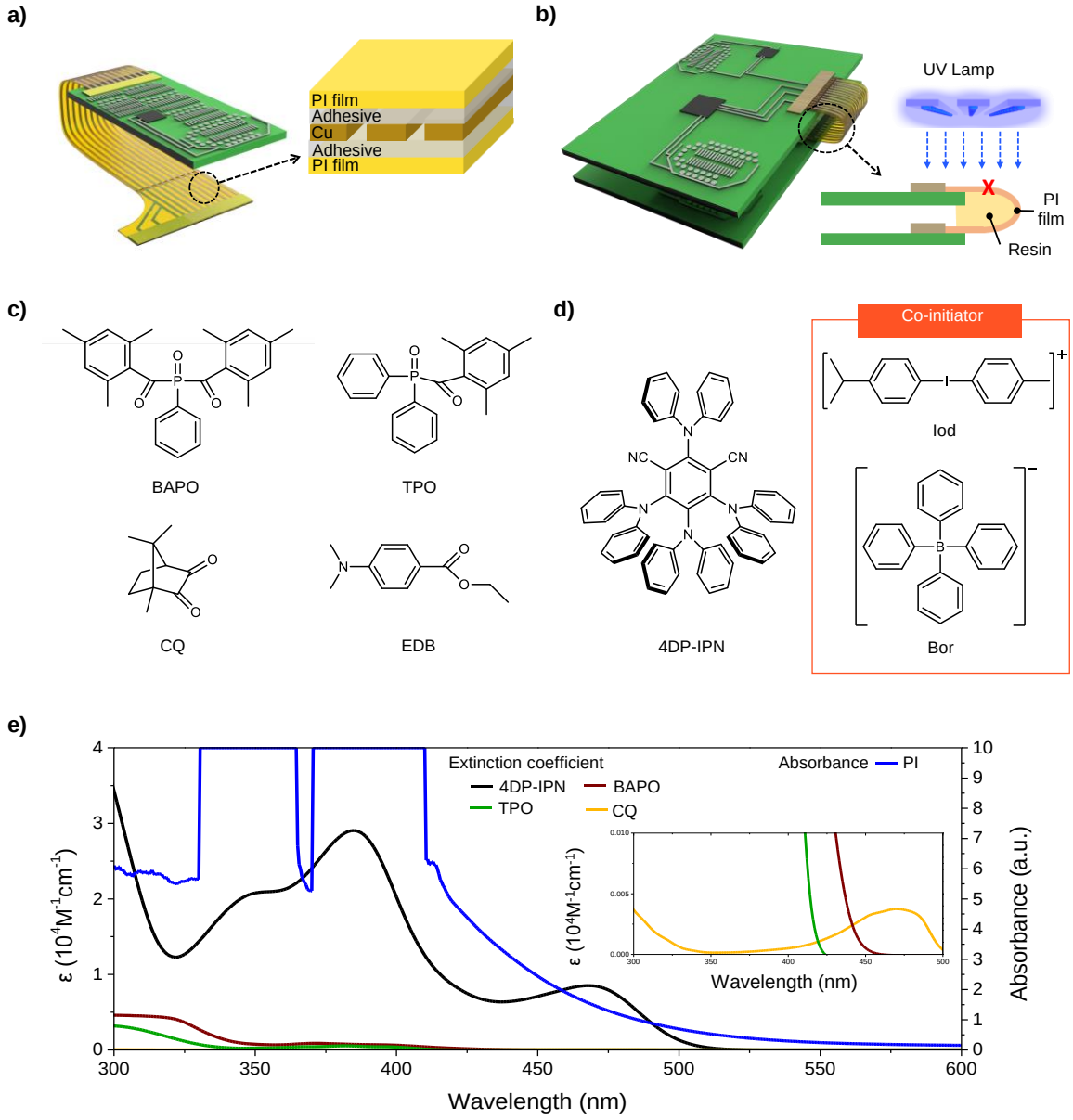

Fig. 1 Schematic overview of this study: a) Structure of FPCB. b) Schematic depiction of the UV curing challenges in the inner resin of FPCB. c) Structures of key Norrish type I visible-light photoinitiators (BAPO and TPO) and Norrish type II photoinitiators (CQ) alongside their co-initiators (EDB). d) Visible-light photoinitiation system featuring photocatalyst 4DP-IPN and co-initiators (iodonium and borate). e) UV-vis absorption spectra of PI films and molar extinction coefficients of the photocatalyst and photoinitiators.

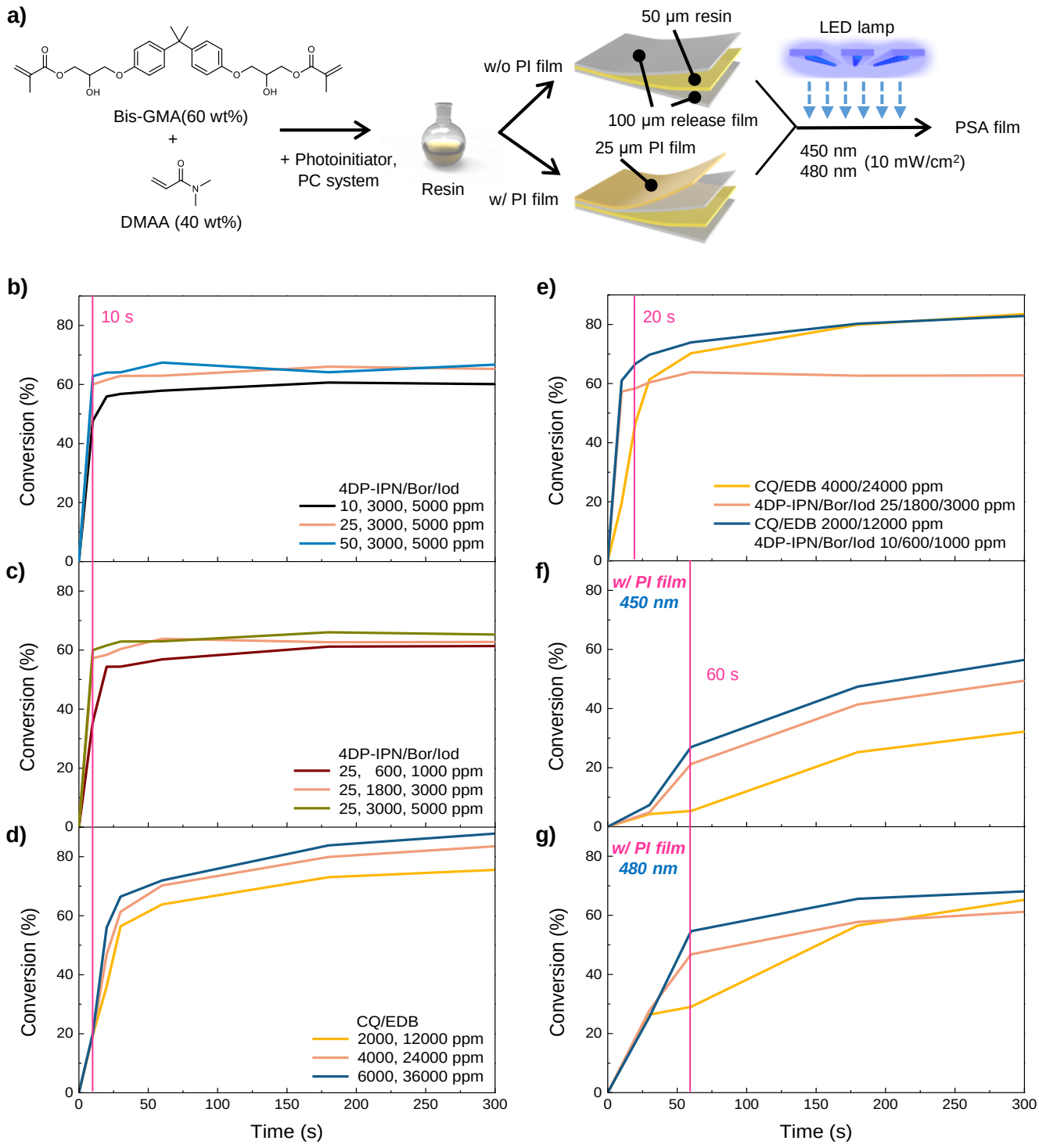

Fig. 2 Evaluation of photocuring under various conditions. a) Schematic illustration of the photocuring process, showcasing different photoinitiation systems, the presence or absence of PI, and varying light irradiation conditions. Resin conversion plots over time at 450 nm, 10 mW/cm², without PI film: b) Influence of PC content in the 4DP-IPN/iodonium/borate system; c) Impact of co-initiators in the 4DP-IPN/iodonium/borate system; d) Effect of varying CQ and EDB concentrations in the CQ/EDB system. Comparative analysis of photocuring performance for the 4DP-IPN/iodonium/borate system, CQ/EDB system, and multicomponent system: e) 10 mW/cm² at 450 nm without PI film; f) 10 mW/cm² at 450 nm with PI film; g) 10 mW/cm² at 480 nm with PI film.

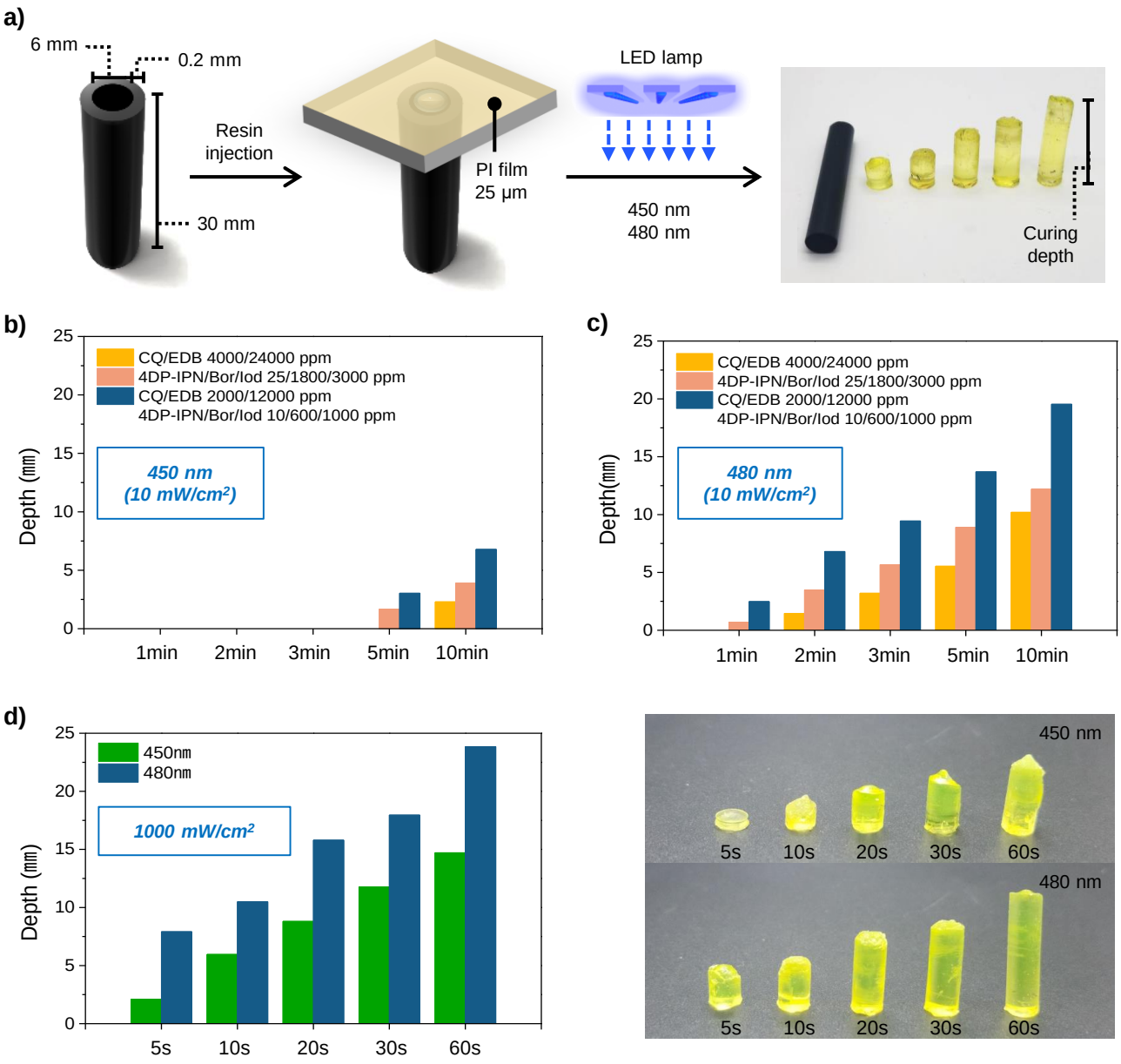

Fig. 3 Resin depth curing assessment. a) Schematic illustration of the depth curing evaluation, using a black tube (30 mm height, 6 mm diameter) filled with resin, covered with a 25 µm PI film, and irradiated with visible light at 450 nm and 480 nm. Depth curing results over time for each photoinitiating system, measured by the length of the cured resin at b) 450 nm, 10 mW/cm², and c) 480 nm, 10 mW/cm². Depth curing results for the multicomponent system over time at d) 450 nm, 1000 mW/cm² (green), and 480 nm, 100 mW/cm² (blue).

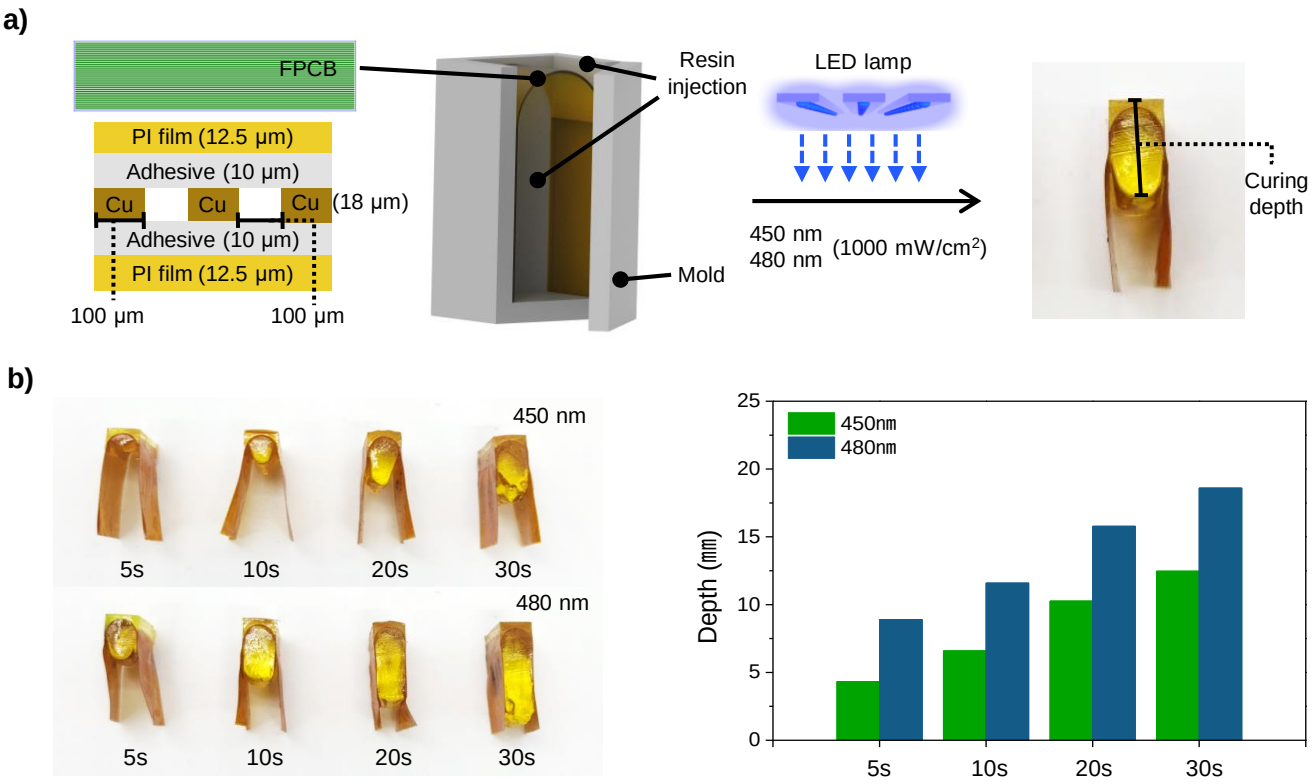

412

413 **Fig. 4 Evaluation of the multicomponent system on actual FPCB.** a) Schematic of the experimental setup for assessing resin
414 cure depth. The FPCB features a layered structure comprising a 12.5 μm PI film, 10 μm adhesive, and 100 μm wide Cu wiring with
415 100 μm spacing. The FPCB was bent and placed in a mold, where resin was injected and applied to the top. The resin was then
416 cured by exposure to 450 nm and 480 nm light at 1000 mW/cm², and the resulting cure depth was measured. b) Resin curing results
417 under 450 nm and 480 nm light at 1000 mW/cm² for varying exposure times.

418

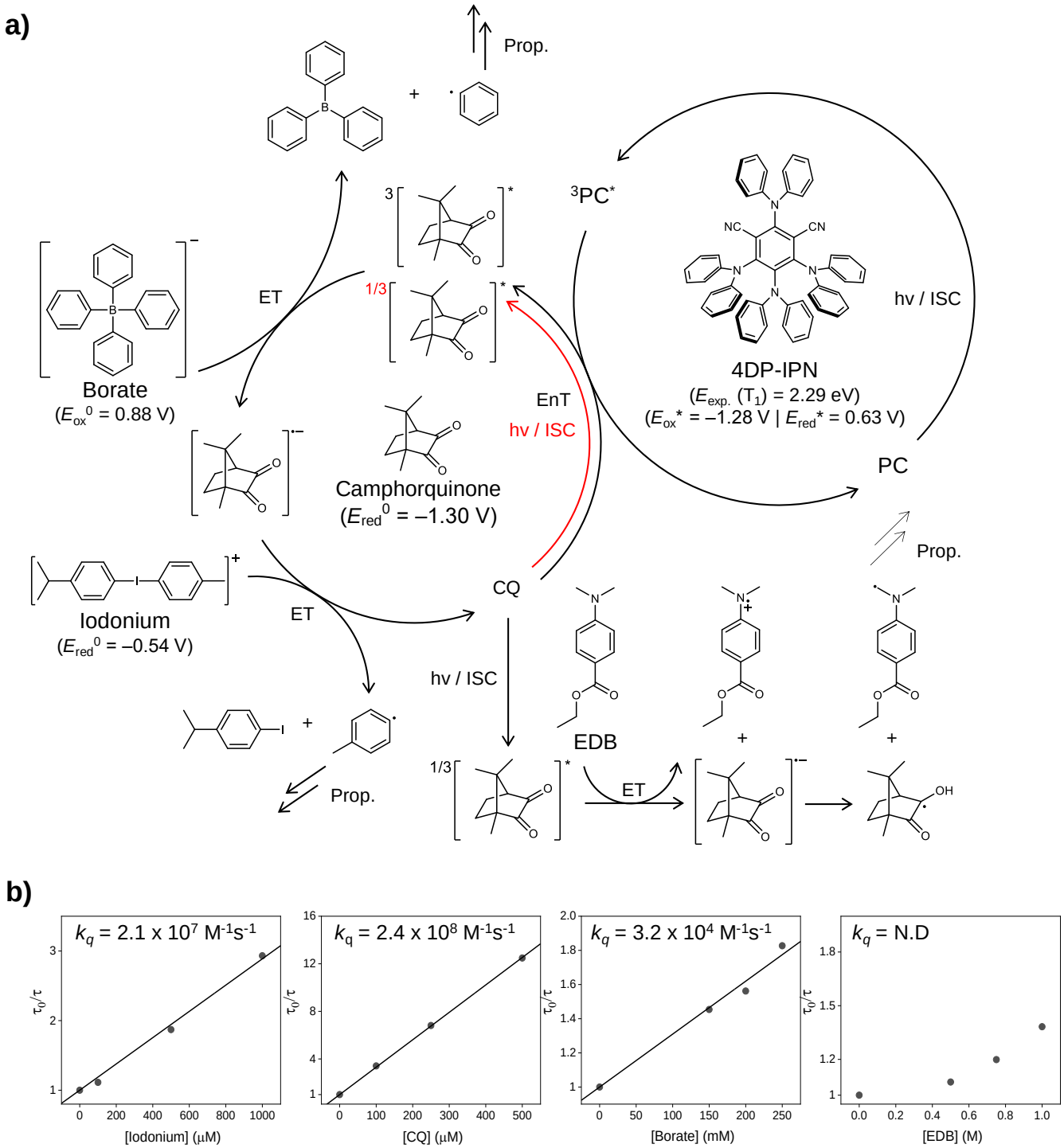

Fig. 5 Mechanistic study of the multicomponent visible-light initiating system. (a) Proposed mechanism of the multicomponent visible-light initiating system. (b) Stern-Volmer plots for delayed fluorescence (DF) quenching in a degassed solution of 4DP-IPN in DMAc (1.0×10^{-5} M) at room temperature, obtained by adding iodonium, camphorquinone, borate, and EDB. Delayed fluorescence decay of 4DP-IPN was monitored using time-correlated single photon counting (TCSPC) techniques at λ_{ex} = 377 nm and λ_{det} = 520 nm.